Geophysical Research Letters

RESEARCH LETTER
10.1029/2022GL102373

Key Points:

- High-resolution 3D LiDAR scans at subsecond intervals demonstrate a novel method for exploring debris-flow dynamics
- LiDAR-derived front and surface velocities allow identification of processes forming and maintaining the debris-flow front
- Observations of individual particle motion place constraints on the vertical velocity profile and temporal variation in flow regimes

Supporting Information:

Supporting Information may be found in the online version of this article.

Correspondence to:

J. Aaron,
jordan.aaron@erdw.ethz.ch

Citation:

Aaron, J., Spielmann, R., McArdell, B. W., & Graf, C. (2023). High-frequency 3D LiDAR measurements of a debris flow: A novel method to investigate the dynamics of full-scale events in the field. *Geophysical Research Letters*, *50*, e2022GL102373. https://doi.org/10.1029/2022GL102373

Received 3 DEC 2022
Accepted 15 FEB 2023

Author Contributions:

Conceptualization: Jordan Aaron, Brian W. McArdell, Christoph Graf
Data curation: Jordan Aaron, Raffaele Spielmann
Formal analysis: Jordan Aaron, Raffaele Spielmann
Funding acquisition: Jordan Aaron, Brian W. McArdell
Investigation: Jordan Aaron, Raffaele Spielmann
Methodology: Jordan Aaron, Raffaele Spielmann, Brian W. McArdell, Christoph Graf
Project Administration: Jordan Aaron

High-Frequency 3D LiDAR Measurements of a Debris Flow: A Novel Method to Investigate the Dynamics of Full-Scale Events in the Field

Jordan Aaron[1,2], Raffaele Spielmann[1,2], Brian W. McArdell[1], and Christoph Graf[1]

[1]Swiss Federal Institute for Forest, Snow and Landscape Research WSL, Birmensdorf, Switzerland, [2]Department of Earth Sciences, Engineering Geology Group, Geological Institute, ETH Zurich, Zurich, Switzerland

Abstract Surging debris flows are among the most destructive natural hazards, and elucidating the interaction between coarse-grained fronts and the trailing liquefied slurry is key to understanding these flows. Here, we describe the application of high-resolution and high-frequency 3D LiDAR data to explore the dynamics of a debris flow at Illgraben, Switzerland. The LiDAR measurements facilitate automated detection of features on the flow surface, and construction of the 3D flow depth and velocity fields through time. Measured surface velocities (2–3 m s^{-1}) are faster than front velocities (0.8–2 m s^{-1}), illustrating the mechanism whereby the flow front is maintained along the channel. Further, we interpret the relative velocity of different particles to infer that the vertical velocity profile varies between plug flow and one that features internal shear. Our measurements provide unique insights into debris-flow motion, and provide the foundation for a more detailed understanding of these hazardous events.

Plain Language Summary Debris flows are surging flows of soil, wood, and water that can impact people and infrastructure far downstream of their initiation zone. Work by others has identified that debris flows tend to develop a distinct segregation between large particles concentrated at the front of the flow and small particles at the tail; however, the formation process and implications of this for debris-flow motion have remained vague. In this work, we present measurements from laser scanners, originally developed for autonomous vehicles, that provide insight into this process. The scanners provide 10 scans per second, which can be used to measure the velocity of objects (rocks and woody debris) on the surface of the flow. We show that different objects in the flow move at different speeds, which results in many destructive features of debris flows. These measurements, and the resulting process understanding, are important for predicting debris-flow hazard and reducing the associated risk.

1. Introduction

Debris flows are extremely rapid surging flows that can reach velocities in excess of 5 m s^{-1}, and travel for thousands of meters (Hungr et al., 2014). Despite decades of research into debris flows, these natural hazards cause costly disasters every year (Andres & Badoux, 2019; Petley, 2012). The destructiveness of debris flows is often amplified by their surging behavior, whereby peak discharge and impact pressure can be highly magnified (e.g., Hungr, 2000; Kean et al., 2016). Previous work has shown that understanding the interaction between coarse components of the flow, often manifest as a boulder-rich front, and a trailing slurry, which is composed of a mixture of soil and water, is critical for understanding this destructive surging behavior (Hungr, 2000; Iverson, 1997; Johnson et al., 2012). One major factor limiting our understanding of this interaction is a lack of high-quality field data that can be used to constrain numerical and physical models. In the present work, we leverage time-lapse LiDAR sensors, originally developed for autonomous vehicles, to estimate critical debris-flow properties at high spatial and temporal resolution, enabling us to analyze debris-flow propagation at the field scale.

Coarse-grained boulder fronts are the product of longitudinal sorting, a mechanism which results in the characteristic grain size of flowing particles varying depending on the position within the flow (Gray, 2018; Gray & Ancey, 2009; Hungr, 2000; Iverson, 1997; Major & Iverson, 1999; McArdell et al., 2007; McCoy et al., 2010; Zhou et al., 2019). This mechanism can also lead to the formation of levees and self-channelization, which restrict lateral spreading and increase runout distances (Gray & Ancey, 2009; Gray & Kokelaar, 2010; Johnson et al., 2012; Kokelaar et al., 2014). Experimental and numerical evidence suggests that coarse fronts are maintained by boul-

Resources: Jordan Aaron
Software: Jordan Aaron, Raffaele Spielmann
Validation: Jordan Aaron
Visualization: Jordan Aaron, Raffaele Spielmann
Writing – original draft: Jordan Aaron
Writing – review & editing: Jordan Aaron, Raffaele Spielmann, Brian W. McArdell, Christoph Graf

der recirculation, whereby coarse particles are continually overrun and recirculated to the front of the flow due to a vertical velocity profile (Gray, 2018; Gray & Kokelaar, 2010; Johnson et al., 2012; Leonardi et al., 2015).

One poorly understood, but key feature of debris flows, is the shape and evolution of this vertical velocity profile. Johnson et al. (2012) discuss two end member velocity profiles; simple shear, which results in a linear velocity profile with no basal slip, and block sliding, whereby all material throughout the depth of the flow moves with the same velocity. Velocity profiles intermediate between these two can occur, either with or without basal slip (Johnson et al., 2012; Nagl et al., 2020). Nagl et al. (2020) provide measurements of the vertical velocity profile from two natural debris flows, and show that it varies from block sliding at the flow front to a more linear profile (approaching simple shear) behind. To the authors knowledge, this is the only work to provide such measurements in natural flows.

Measurements of in situ debris-flow properties are relatively rare, but they have been collected in a few locations (e.g., Hürlimann et al., 2019). These have included surface measurements of flow depth and velocity, as well as basal measurements of pore pressures, normal, and shear forces. Further, surface velocity measurements in experiments have revealed that the flow front tends to be moving slower than the liquefied slurry behind, which has implications for longitudinal sorting (Arai et al., 2013; Huebl & Kaitna, 2021; Johnson et al., 2012), although this has yet to be confirmed at the field scale. Laser scanning and video analysis have been used at some field locations and in large-scale experiments, although some of these methods have limited temporal and/or spatial resolution (Jacquemart et al., 2017; Osaka et al., 2013; Rapstine et al., 2020; Rengers et al., 2021; Theule et al., 2018; Uddin et al., 1998).

There is thus a gap between linking experimental and numerical studies to debris-flow movement mechanisms in the field. In particular, high-resolution field measurements of front and surface velocity fields, longitudinal and lateral variations in flow depth, as well as boulder trajectories are required to further our understanding of debris-flow motion. Here, we present a new sensor array and data processing methodology for in situ measurements of key debris-flow parameters that is able to fill this gap.

2. Site Overview

Our sensor array is installed in the Illgraben Debris-Flow Monitoring Station, located in the Canton of Valais in south-western Switzerland. The station has been in operation since the year 2000, and records properties of 2–10 debris flows every year (Badoux et al., 2009; Bennett et al., 2013; Berger et al., 2011; Hürlimann et al., 2003; McArdell, 2016; McArdell et al., 2007; Schürch et al., 2011). This in situ laboratory contains a geophone array to estimate flow front velocity and provide trigger signals for data loggers, radar, ultrasonic, and laser devices to determine flow depth, a force plate to measure normal and shear forces, and multiple video cameras. We captured a debris-flow event that occurred on 19 September 2021, and lasted for ∼30 min (Figure 1, Figure S1 in Supporting Information S1, Movies S1 and S2).

3. Materials and Methods

We installed a high-resolution Light Detection and Ranging (LiDAR) scanner in the Illgraben to record point clouds of the debris-flow surface at high temporal and spatial resolution (Figure 1). This scanner (Ouster OS1-64 Gen. 1) has a 33.5° field of view and a spatial resolution of 64 scan lines. It was set to a resolution of 10 Hz and 2,048 points per line. The LiDAR unit is mounted 6 m above a check dam in the middle of the channel (Figures 1 and S2 in the Supporting Information S1), and is triggered by an upstream geophone.

3.1. Feature Detection and Tracking

We manually derived positions and velocities of features in the LiDAR data using the Matlab toolbox "groundTruthLabeler" to draw 3D bounding boxes around features in the point cloud. We classified each feature as either woody debris, a floating boulder, or a rolling boulder (Figure 1).

We use the number of features that can be visually distinguished on the surface of the flow in the video imagery as a proxy for the concentration of coarse-grained particles (down to ∼20-cm diameter) present in the flow. To quantify this proxy, we trained a convolutional neural network (CNN) to detect boulders and woody debris in

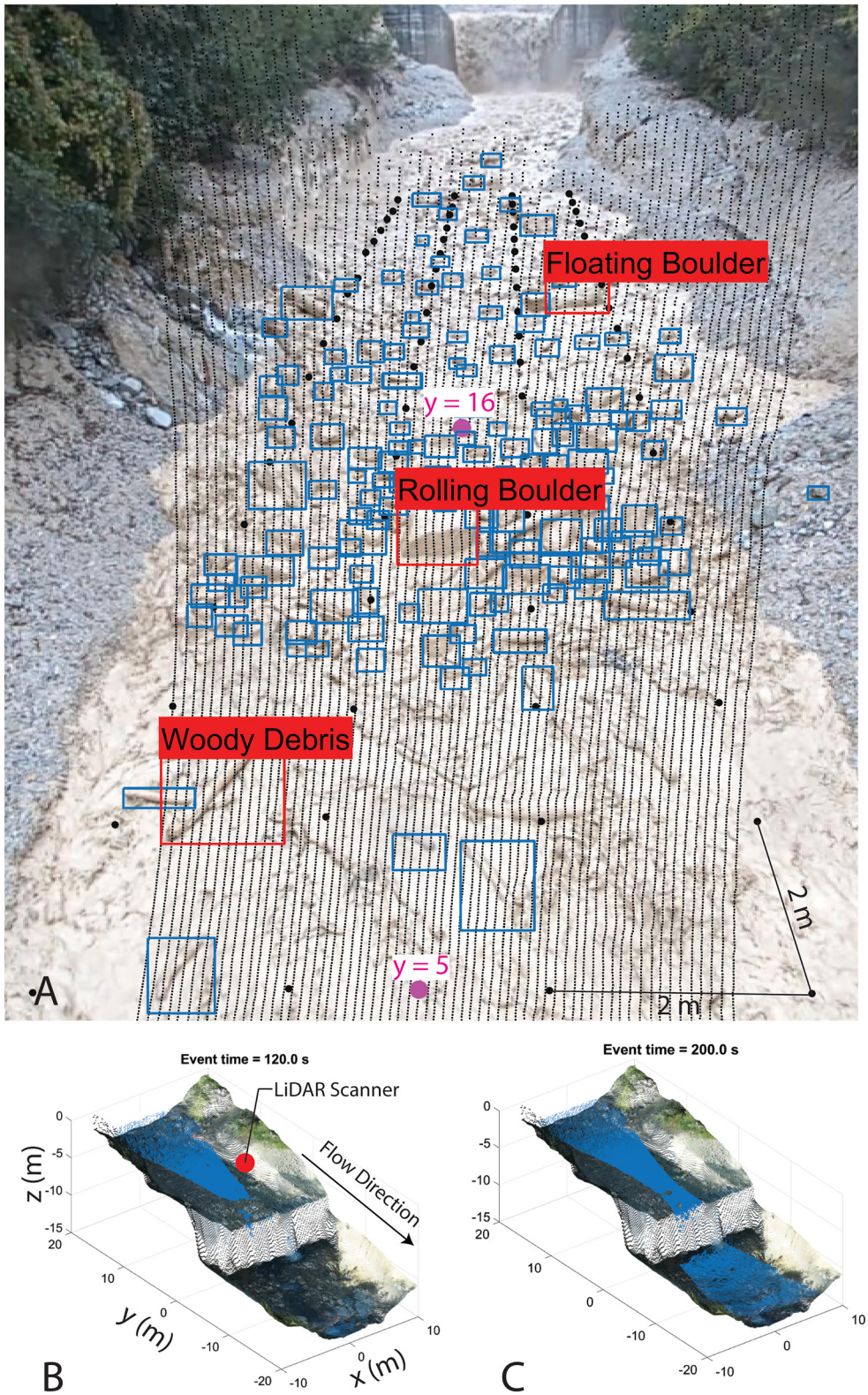

Figure 1.

our video imagery, based on a labeled data set of images (Figure S3 in Supporting Information S1). We used an off-the-shelf implementation of YOLO-v5 (Redmon et al., 2016), and trained it with feature labels manually drawn using the open-source tool "LabelImg" (Tzutalin, 2015). Our CNN achieved a test-set precision of 0.8, and recall of 0.6. Example detections are shown in Figure 1 and Figure S4 in the Supporting Information S1.

3.2. Automated Velocity Estimation

We developed two methods to automatically generate continuous time series of front and surface velocities, based on the collected point cloud and video data. One is based on hillshade projections of the point clouds, and the other on fusing the camera and LiDAR data. For the hillshade method, the point cloud was first fit using a triangular interpolant, and then rasterized to a constant 5-cm resolution. The hillshade projection function given by Wenbin (2022) was then used to generate a hillshade for each time step (see Movie S3). The hillshade images were then analyzed using particle image velocimetry (PIV), as implemented by PIV-Lab (Thielicke & Sonntag, 2021), to derive a dense 2D velocity field based on matching features in one LiDAR frame to a subsequent frame captured 1/10 of a second later. This 2D velocity field was subsequently projected onto the LiDAR data to obtain 3D velocities, as described in the Supporting Information S1.

For the LiDAR-camera fusion method, we applied PIV to the video data, and then obtain 3D velocity fields as described in the Supporting Information S1. This required us to estimate the transformation between the LiDAR and camera, which was done using an adaptation of the method presented in Huang and Grizzle (2020). Figure 1 shows an example of the LiDAR data projected onto the camera imagery. Figures S5–S9 in the Supporting Information S1 show example results and a validation of the automated velocity methods. All automated velocities presented here were smoothed with a 2 s moving mean.

3.3. Flow Depth and Front Trajectory

We estimate vertical flow depths by differencing the instantaneous LiDAR scan data with the pre-event channel-bed surface elevation. Flow depth estimation is complicated because we only measure the top surface, and do not know the position of the base of the debris flow due to erosion and deposition during the event (e.g., Berger et al., 2011). There is thus an unknown error caused by erosion/deposition during flow, which may be somewhat mitigated by the presence of the check dam, which stabilizes the channel bed.

We further process the flow depth data to identify the trajectory of the flow front through the study reach. We extract velocities of the front position from the vector field that results from the automated methods detailed above, as well as the surface velocities of material 2, 6, and 10 m behind the front. This was done approximately every 2 s, to ensure that the front could be clearly identified. By comparing these velocities, we are able to quantify the front propagation process.

4. Results

The results over a 30-m long reach of channel upstream of the check dam indicate that the flow is highly non-uniform and unsteady. The front velocity varies from ∼2 m s^{-1} down to ∼0.8 m s^{-1} near the check dam, in agreement with manual mapping of the front position (Figure 2a). The material behind the front moves with a consistently larger velocity than the front, and material slows down as it reaches the front. The ratio between the surface velocity 6 and 10 m behind the front and the front velocity varies from ∼1 to 2 (Figure 2b), with a sharp increase when the front decelerates as it approaches the check dam (between ∼01:53 and 01:55 in Figure 2a, i.e., 6–7 m upstream of the sensor, see Figure 1). In this segment, the channel cross section widens, and a cross-channel surface velocity gradient develops, which leads to the deposition of levees, which are subsequently remobilized (Movie S2). Figure 2c shows the instantaneous surface position and velocities of the debris flow at t = 01:48 min. Detailed analysis of the point cloud and video data show that the front is composed of boulders that define the local flow depth (Movies S5 and S6). We are able to track these boulders for the full 30 m channel section (Movie S2), suggesting that they are not being recirculated.

Figure 1. (a) Video frame from the 19 September 2021 event. The blue boxes show the convolutional neural network (CNN) detections, the red boxes show the three manually labeled feature types, the small black dots show the Light Detection and Ranging (LiDAR) scan projected onto the image, and the magenta dots show the location of point measurements of flow depth and velocity. The large black dots show a 2 × 2 m grid projected onto the image. (b) and (c) show the point cloud frames (blue dots) overlain on a post-event UAV digital elevation model at times 120 and 200 s, respectively (de Haas et al., 2022). The check dam can be seen as the white step at $\sim y = 0$.

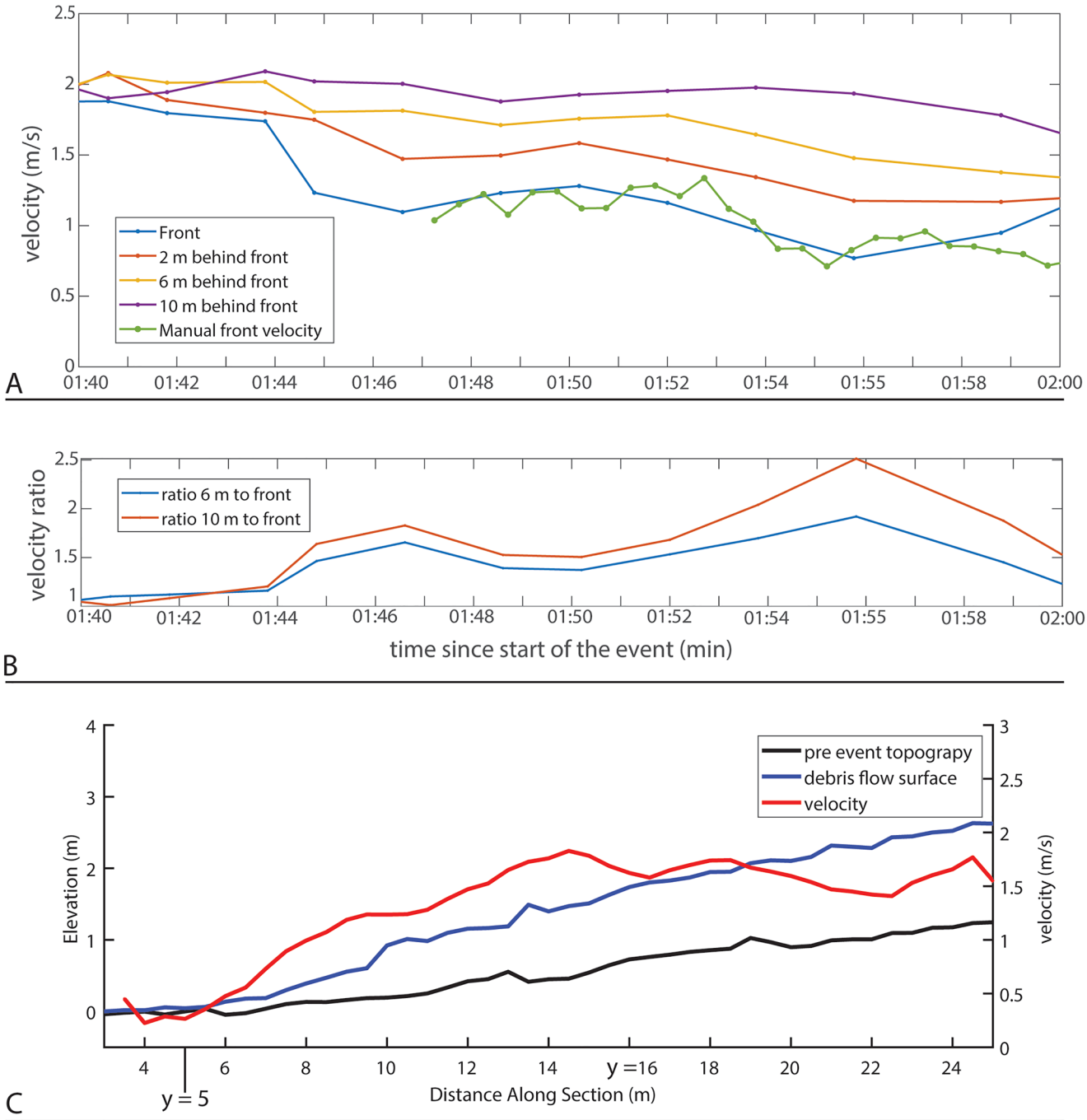

Figure 2. Velocity variation within the debris-flow front along the centerline of the flow. (a) Front and surface velocity evolution through time, derived from the hillshade-based method and manual measurements (see text). (b) Ratio of surface velocity at 6 and 10 m upstream of the front to the front velocity. (c) Longitudinal section of the flow upstream of the sensor at 01:48 min, also showing the preevent channel-bed topography, corresponding surface velocities, and locations of the point measurements shown in Figure 3. Note that the elevation is vertically exaggerated.

Following the arrival of the front, we analyze surface velocities, flow depths, and number of boulders at the surface of the debris flow (Figures 3 and 4). The flow depth builds to a maximum of 1.5 m once the front has passed, and then progressively decreases, accompanied by a corresponding decrease in velocity and number of boulder detections (compare to Figure 4). Furthermore, we observe a pronounced decrease in flow depth from $y = 16$ m to $y = 5$ m, i.e., toward the check dam (located at approximately $y = -2.5$ m; Figure 1).

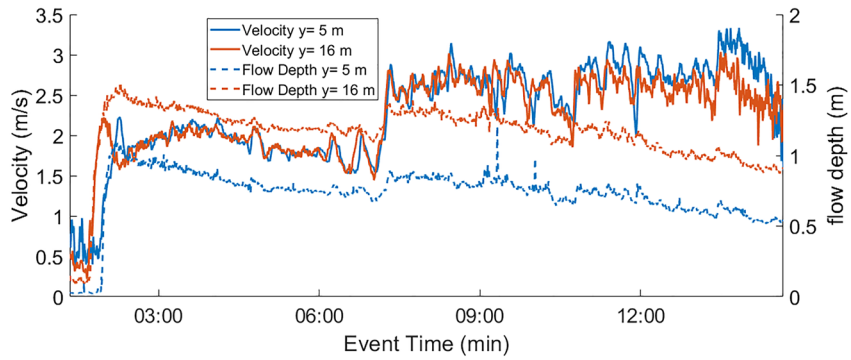

Figure 3. Comparison of hillshade derived surface velocity and flow depth at various locations through time. The numbers in the figure legend correspond to the distance (m) upstream of the sensor (see also Figure 1).

Approximately 7 min into the event, Figure 3 shows a second increase in flow depth over a 15-s period along with a corresponding increase in velocities (referred to as the "velocity jump" below). The arrival of this second surge occurs abruptly ~2 min after boulder detections have fallen to a minimum (Figure 4a).

We manually mapped 29 features on the surface of the moving debris flow, which included 9 woody debris features and 20 rolling boulders (Figure 4a). Prior to the velocity jump, rolling boulders and woody debris tend

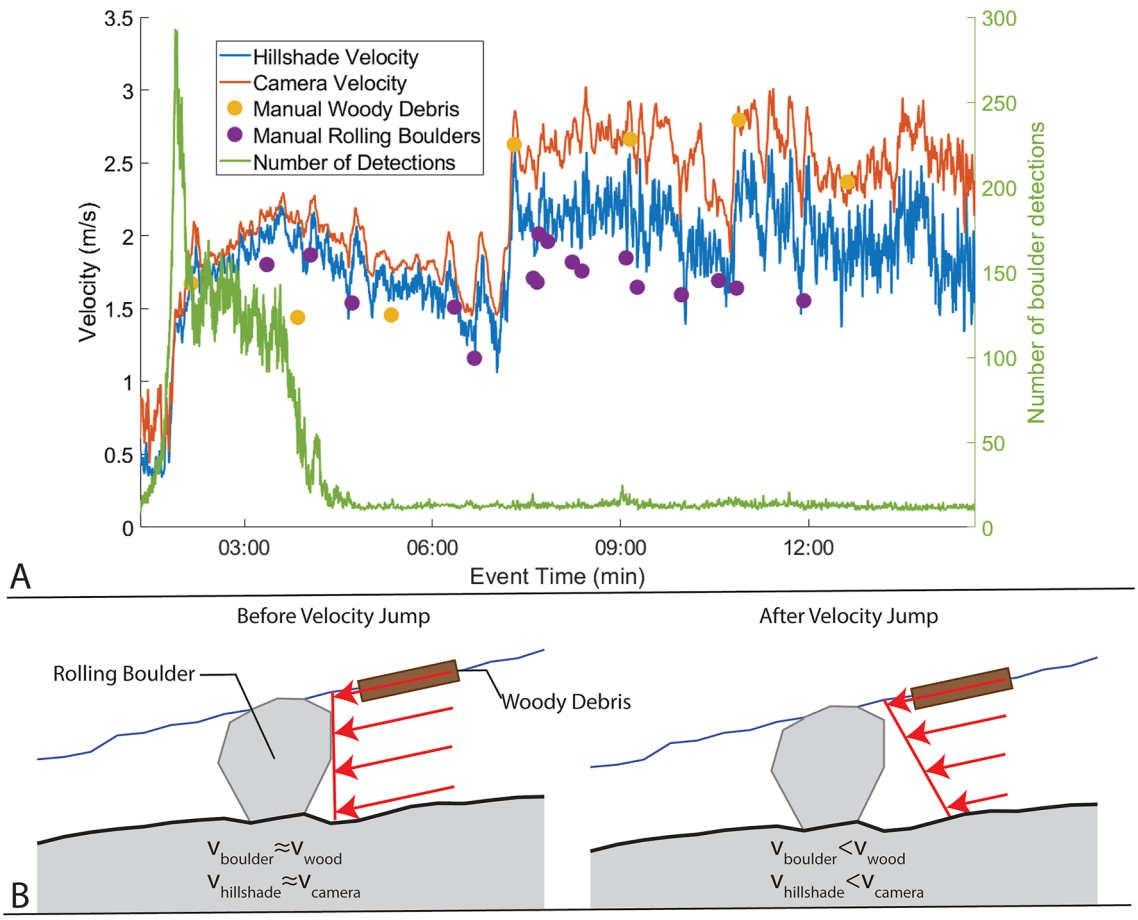

Figure 4. (a) Velocities of features on the surface of the flow derived from manual mapping and automated velocity measurements (mean in channel segment from 8 to 11 m upstream of sensor) as described in the text. The number of large boulder detections from the convolutional neural network (CNN) can also be seen. (b) Interpreted debris-flow vertical velocity profile before and after the velocity jump (roughly at 07:00; as described in text), with different features shown schematically. We note that our measurements cannot estimate the relative proportion of basal slip, but they indicate that there is internal shear either with or without basal slip (see also Section 1).

to move at a similar velocity, whereas after the jump these two velocities strongly diverge, with rolling boulders moving at ~0.6–0.7× the velocity of woody debris (Figure 4a). The automatically calculated velocities are consistent with this observation, with the two methods diverging at the velocity jump (Figure 4a). The hillshade method more accurately matches the manual observations of rolling boulder velocity, whereas the camera method more accurately matches the manually derived woody debris velocity (Figure 4a and Figures S5, S7 in the Supporting Information S1). As discussed in the following section, this has important implications for understanding the temporal evolution of the vertical velocity profile (Figure 4b).

5. Discussion

Debris flows are frequent natural hazards whose destructiveness is strongly controlled by their surging behavior. While many theories have been proposed to explain the formation and propagation of debris-flow surges, few measurements of debris-flow front and surface velocity, flow depth and particle positions have been reported at high temporal and spatial resolution (e.g., Hürlimann et al., 2019). In the present work, we proposed a new suite of methods based on LiDAR scanning technology, the fusion of LiDAR and video recordings, and deep learning-based particle-detection methods which help to close this methodological gap. We then demonstrated the application of these new methods for one debris flow observed at Illgraben.

Our new methods enabled us to derive high spatial and temporal resolution front and surface velocity and flow depths fields. Further, we derived and classified the trajectories of features visible on the flow surface using subsecond sampling. Our methods result in an over 1 order of magnitude increase in the spatial resolution that the above mentioned parameters have been measured at, compared to previous work (e.g., Hürlimann et al., 2019; Jacquemart et al., 2017). We are thus able to gain a new perspective on debris-flow motion, and use these data to infer information regarding front maintenance and propagation, surge development, and the vertical velocity profile.

We described front and surface velocities over a 30-m long section of the channel, and compared both to understand the motion of particles within the flow that help to maintain the boulder-rich front as well as its propagation over the channel bed. Surface velocities behind the propagating front exceeded the front velocity (Figure 2) by a factor of 1.5, indicating preferential movement of boulders to the front of the flow. We have thus directly quantified the rates of particle movement that maintain the bouldery front of the flow.

We tracked the position of individual particles over tens of meters throughout the duration of the flow (Figure 4a, Movies S2 and S4). We find that, while front and surface velocities differ (Figure 2), boulder recirculation does not occur. Particles on the surface decelerate as they approach the front (Figure 2), and remain as part of the front once it is reached, or are shouldered aside to form levees. This is in contrast to experimental (Johnson et al., 2012) and numerical studies (Gray, 2018), and suggests that boulder front propagation does not always require boulder recirculation.

The likely difference between the 19 September 2021 event and these past studies is that in our event the size of boulders at the front are the same as the local flow depth. These boulders retained material behind them, and we hypothesize that this caused the front to act as a sieve (and not a dam), which let water and more fine grained particles escape. This observation is consistent with and helps explain the formation of a precursory surge of fine-sediment-laden water which is typically observed downstream of the bouldery front (Pierson, 1986, Movie S2).

The automatic flow velocity estimates show that a second surge arrives ~7 min into the event, with a corresponding small increase in flow depth (Figures 3 and 4). Visual assessment of the flow (Movie S2), as well as the neural network results (Figure 4a) do not reveal a significant change in the material composition that corresponds to the arrival of this second surge. Instead, we suggest that a subtle change in the material composition and/or water content led to this abrupt change. High sensitivities of debris-flow behavior to subtle changes in water content have been measured in experiments (Kaitna et al., 2016).

Our manual estimates of surface velocity (Figure 4a) suggest that the surface of the measured debris flow does not have a single velocity. This surface is composed of features (cobbles, boulders, and trees) which have variable sizes, and extend to different flow depths (Figure 4b). Our interpretation is that the features sample the vertical velocity profile at different depths, and are thus providing information regarding its shape and temporal evolution

(Figure 4b). Prior to the velocity jump, manual, and automated velocity measurements are consistent with a block-sliding vertical velocity profile (Figures 4a and 4b). However, following the arrival of the second surge, large boulders move significantly slower than woody debris, and the two automatic methods diverge, indicating that the vertical velocity profile features internal shear (Figure 4b). Thus, our measurements are consistent with a change in the vertical velocity profile occurring during the second surge, similar to that reported by Nagl et al. (2020) for two debris-flow events.

Our LiDAR data further show that the change in the velocity profile occurs over a period on the order of 15–30 s. The ratio of 0.6–0.7 after the velocity jump between rolling boulders and woody debris is intermediate between that expected for simple shear (0.5) and that expected for block sliding (1.0). We thus interpret this ratio to indicate that the shape of the vertical velocity profile must be between these two end-members (Figure 4b). Our results further suggest that the transition between the two is abrupt, and likely influenced by the concentration of coarse particles. Coarse particles, whose size approaches the local flow depth, suppress the development of a vertical velocity profile because they are too large to allow vertical shearing. Further, and as described above, changes in water content likely also contributed to this abrupt change in debris-flow behavior. Additional observations are necessary to confirm the generality of this result, but it suggests that particle size and sorting is an important control on debris-flow dynamics, as has been demonstrated in other studies (e.g., Gray, 2018).

We further measure a pronounced decrease in flow depth as the flow approaches the check dam (Figure 3). This is likely caused by a hydraulic drawdown effect, as is observed for open channel flows in river channels (e.g., Henderson, 1966). This effect is important to account for when interpreting data from measurement stations near check dams, as the flow depth is significantly influenced for ∼15 m upstream. We expect that this effect will be Froude number dependent, and data from future events will help to further explore this.

Our results have highlighted the variable nature of debris-flow dynamics over short time scales, and suggest that the concentrations of coarse particles can influence the vertical velocity profile of the flow, leading to different flow regimes occurring within a single event. Furthermore, our results suggest that boulders at the front of the flow do not need to be recirculated in order for a boulder front to persist. Instead, we hypothesize that the coarse-grained boulder front may lead to drainage of pore pressures, resulting in a velocity decrease as boulders approach the front. These boulders are then pushed by the trailing material, and move with a combination of rolling and sliding kinematics. Data from future events, recorded with the same monitoring system, will help to further elucidate these processes.

6. Conclusions

Using a new high-sampling frequency 3D LiDAR scanner, we have recorded high spatial and temporal resolution point clouds of a debris flow, and analyzed these data to understand debris-flow dynamics. We show that front velocities are consistently slower than surface velocities of the trailing material, which moves ∼1.5 to 2× faster than the front in the present event. Boulders slow down as they reach the front and are not recirculated, but instead move through a combination of rolling and sliding. Following the passage of the front, our interpretation suggests that boulder concentrations decrease until the vertical velocity profile of the flow abruptly changes from block sliding to one that features internal shearing. These results have implications for understanding and predicting debris-flow motion, which is critical for managing the hazard posed by these events. In particular, the interaction between coarse particles in the flow and the trailing slurry appears to result in different flow regimes occurring at different times throughout the flow. Data from future events will help to further clarify the generality of these results.

Data Availability Statement

The workflow used in this project is based on the following open-source software:

- PIV-Lab https://www.mathworks.com/matlabcentral/fileexchange/27659-pivlab-particle-image-velocimetry-piv-tool-with-gui (Thielicke & Sonntag, 2021).
- Yolo-v5 https://github.com/ultralytics/yolov5 (Redmon et al., 2016).
- LabelImg https://github.com/heartexlabs/labelImg (Tzutalin, 2015).
- Hillshade Function: https://www.mathworks.com/matlabcentral/fileexchange/32088-esri-hillshade-algorithm (Wenbin, 2022).

The point cloud and imagery data used in this study can be found here: https://doi.org/10.3929/ethz-b-000599948.

Acknowledgments
This project was funded by an SNSF Ambizione Grant 193081 to J. Aaron, as well as funds from the Chair of Engineering Geology at ETH Zurich. We are grateful for technical support from Stefan Boss, as well as assistance with boulder labeling from Sebastian Harder and Melissa Kundert. We thank Professor Tjalling de Haas for providing the UAV data used in this study. Finally, we thank Roland Kaitna and Francis Rengers for thorough and constructive reviews that greatly improved the manuscript.

References

Andres, N., & Badoux, A. (2019). The Swiss flood and landslide damage database: Normalisation and trends. *Journal of Flood Risk Management*, *12*(S1), 913–925. https://doi.org/10.1111/jfr3.12510

Arai, M., Huebl, J., & Kaitna, R. (2013). Occurrence conditions of roll waves for three grain-fluid models and comparison with results from experiments and field observation. *Geophysical Journal International*, *195*(3), 1464–1480. https://doi.org/10.1093/gji/ggt352

Badoux, A., Graf, C., Rhyner, J., Kuntner, R., & McArdell, B. W. (2009). A debris-flow alarm system for the Alpine Illgraben catchment: Design and performance. *Natural Hazards*, *49*(3), 517–539. https://doi.org/10.1007/s11069-008-9303-x

Bennett, G. L., Molnar, P., McArdell, B. W., Schlunegger, F., & Burlando, P. (2013). Patterns and controls of sediment production, transfer and yield in the Illgraben. *Geomorphology*, *188*, 68–82. https://doi.org/10.1016/j.geomorph.2012.11.029

Berger, C., McArdell, B. W., & Schlunegger, F. (2011). Sediment transfer patterns at the Illgraben catchment, Switzerland: Implications for the time scales of debris flow activities. *Geomorphology*, *125*(3), 421–432. https://doi.org/10.1016/j.geomorph.2010.10.019

de Haas, T., McArdell, B. W., Nijland, W., Åberg, A. S., Hirschberg, J., & Huguenin, P. (2022). Flow and bed conditions jointly control debris-flow erosion and bulking. *Geophysical Research Letters*, *49*, e2021GL097611. https://doi.org/10.1029/2021GL097611

Gray, J. M. N. T. (2018). Particle segregation in dense granular flows. *Annual Review of Fluid Mechanics*, *50*(1), 407–433. https://doi.org/10.1146/annurev-fluid-122316-045201

Gray, J. M. N. T., & Ancey, C. (2009). Segregation, recirculation and deposition of coarse particles near two-dimensional avalanche fronts. *Journal of Fluid Mechanics*, *629*, 387–423. https://doi.org/10.1017/S0022112009006466

Gray, J. M. N. T., & Kokelaar, B. P. (2010). Large particle segregation, transport and accumulation in granular free-surface flows. *Journal of Fluid Mechanics*, *652*, 105–137. https://doi.org/10.1017/S002211201000011X

Henderson, F. M. (1966). *Open channel flow*. Macmillan.

Huang, J.-K., & Grizzle, J. W. (2020). Improvements to target-based 3D LiDAR to camera calibration. *IEEE Access*, *8*, 134101–134110. https://doi.org/10.1109/ACCESS.2020.3010734

Huebl, J., & Kaitna, R. (2021). Monitoring debris-flow surges and triggering rainfall at the Lattenbach Creek, Austria. *Environmental and Engineering Geoscience*, *27*(2), 213–220. https://doi.org/10.2113/EEG-D-20-00010

Hungr, O. (2000). Analysis of debris flow surges using the theory of uniformly progressive flow. *Earth Surface Processes and Landforms*, *25*(5), 483–495. https://doi.org/10.1002/(SICI)1096-9837(200005)25:5<483::AID-ESP76>3.3.CO;2-Q

Hungr, O., Leroueil, S., & Picarelli, L. (2014). The Varnes classification of landslide types, an update. *Landslides*, *11*(2), 167–194. https://doi.org/10.1007/s10346-013-0436-y

Hürlimann, M., Coviello, V., Bel, C., Guo, X., Berti, M., Graf, C., et al. (2019). Debris-flow monitoring and warning: Review and examples. *Earth-Science Reviews*, *199*, 102981. https://doi.org/10.1016/j.earscirev.2019.102981

Hürlimann, M., Rickenmann, D., & Graf, C. (2003). Field and monitoring data of debris-flow events in the Swiss Alps. *Canadian Geotechnical Journal*, *40*(1), 161–175. https://doi.org/10.1139/t02-087

Iverson, R. M. (1997). The physics of debris flows. *Reviews of Geophysics*, *35*(3), 245–296. https://doi.org/10.1029/97RG00426

Jacquemart, M., Meier, L., Graf, C., & Morsdorf, F. (2017). 3D dynamics of debris flows quantified at sub-second intervals from laser profiles. *Natural Hazards*, *89*(2), 785–800. https://doi.org/10.1007/s11069-017-2993-1

Johnson, C. G., Kokelaar, B. P., Iverson, R. M., Logan, M., Lahusen, R. G., & Gray, J. M. N. T. (2012). Grain-size segregation and levee formation in geophysical mass flows. *Journal of Geophysical Research*, *117*, F01032. https://doi.org/10.1029/2011JF002185

Kaitna, R., Palucis, M. C., Yohannes, B., Hill, K. M., & Dietrich, W. E. (2016). Journal of geophysical research: Earth surface behavior in experimental debris flows. *Journal of Geophysical Research: Earth Surface*, *121*, 2298–2317. https://doi.org/10.1002/2015JF003725

Kean, J. W., McGuire, L. A., Rengers, F. K., Smith, J. B., & Staley, D. M. (2016). Amplification of postwildfire peak flow by debris. *Geophysical Research Letters*, *43*, 8545–8553. https://doi.org/10.1002/2016GL069661

Kokelaar, B. P., Graham, R. L., Gray, J. M. N. T., & Vallance, J. W. (2014). Fine-grained linings of leveed channels facilitate runout of granular flows. *Earth and Planetary Science Letters*, *385*, 172–180. https://doi.org/10.1016/j.epsl.2013.10.043

Leonardi, A., Cabrera, M., Wittel, F. K., Kaitna, R., Mendoza, M., Wu, W., & Herrmann, H. J. (2015). Granular-front formation in free-surface flow of concentrated suspensions. *Physical Review E-Statistical, Nonlinear and Soft Matter Physics*, *92*(5), 1–13. https://doi.org/10.1103/PhysRevE.92.052204

Major, J. J., & Iverson, R. M. (1999). Debris-flow deposition: Effects of pore-fluid pressure and friction concentrated at flow margins. *Bulletin of the Geological Society of America*, *111*(10), 1424–1434. https://doi.org/10.1130/0016-7606(1999)111<1424:DFDEOP>2.3.CO;2

McArdell, B. W. (2016). Field measurements of forces in debris flows at the Illgraben: Implications for channel-bed erosion. *International Journal of Erosion Control Engineering*, *9*(4), 194–198. https://doi.org/10.13101/ijece.9.194

McArdell, B. W., Bartelt, P., & Kowalski, J. (2007). Field observations of basal forces and fluid pore pressure in a debris flow. *Geophysical Research Letters*, *34*, L07406. https://doi.org/10.1029/2006GL029183

McCoy, S. W., Kean, J. W., Coe, J. A., Staley, D. M., Wasklewicz, T. A., & Tucker, G. E. (2010). Evolution of a natural debris flow: In situ measurements of flow dynamics, video imagery, and terrestrial laser scanning. *Geology*, *38*(8), 735–738. https://doi.org/10.1130/G30928.1

Nagl, G., Hübl, J., & Kaitna, R. (2020). Velocity profiles and basal stresses in natural debris flows. *Earth Surface Processes and Landforms*, *45*(8), 1764–1776. https://doi.org/10.1002/esp.4844

Osaka, T., Takahashi, E., Kunitomo, M., Yamakoshi, T., Nowa, Y., Kisa, H., et al. (2013). Field observations of unit weight of flowing debris flows by force plate in Sakurajima, Japan. *Journal of the Japan Society of Erosion Control Engineering*, *65*(6), 46–50. https://doi.org/10.11475/sabo.65.6_46

Petley, D. (2012). Global patterns of loss of life from landslides. *Geology*, *40*(10), 927–930. https://doi.org/10.1130/G33217.1

Pierson, T. C. (1986). Flow behavior of channelized debris flows, Mount St. Helens, Washington. In *Hillslope processes*. Routledge.

Rapstine, T. D., Rengers, F. K., Allstadt, K. E., Iverson, R. M., Smith, J. B., Obryk, M. K., et al. (2020). Reconstructing the velocity and deformation of a rapid landslide using multiview video. *Journal of Geophysical Research: Earth Surface*, *125*, e2019JF005348. https://doi.org/10.1029/2019JF005348

Redmon, J., Divvala, S., Girshick, R., & Farhadi, A. (2016). You only look once: Unified, real-time object detection. In *2016 IEEE Conference on Computer Vision and Pattern Recognition (CVPR)* (pp. 779–788). https://doi.org/10.1109/CVPR.2016.91

Rengers, F. K., Rapstine, T. D., Olsen, M., Allstadt, K. E., Iverson, R. M., Leshchinsky, B., et al. (2021). Using high sample rate LiDAR to measure debris-flow velocity and surface geometry. *Environmental and Engineering Geoscience*, *27*(1), 113–126. https://doi.org/10.2113/EEG-D-20-00045

Schürch, P., Densmore, A. L., Rosser, N. J., Lim, M., & Mcardell, B. W. (2011). Detection of surface change in complex topography using terrestrial laser scanning: Application to the Illgraben debris-flow channel. *Earth Surface Processes and Landforms*, *36*(14), 1847–1859. https://doi.org/10.1002/esp.2206

Theule, J. I., Crema, S., Marchi, L., Cavalli, M., & Comiti, F. (2018). Exploiting LSPIV to assess debris-flow velocities in the field. *Natural Hazards and Earth System Sciences*, *18*(1), 1–13. https://doi.org/10.5194/nhess-18-1-2018

Thielicke, W., & Sonntag, R. (2021). Particle image velocimetry for MATLAB: Accuracy and enhanced algorithms in PIVlab. *Journal of Open Research Software*, *9*(1), 12. https://doi.org/10.5334/jors.334

Tzutalin (2015). LabelImg. Retrieved from https://github.com/tzutalin/labelImg

Uddin, M. S., Inaba, H., Itakura, Y., & Kasahara, M. (1998). Estimation of the surface velocity of debris flow with computer-based spatial filtering. *Applied Optics*, *37*(26), 6234. https://doi.org/10.1364/AO.37.006234

Wenbin (2022). *Esri hillshade algorithm*. MATLAB Central File Exchange. Retrieved from https://www.mathworks.com/matlabcentral/fileexchange/32088-esri-hillshade-algorithm

Zhou, G. G. D., Li, S., Song, D., Choi, C. E., & Chen, X. (2019). Depositional mechanisms and morphology of debris flow: Physical modelling. *Landslides*, *16*(2), 315–332. https://doi.org/10.1007/s10346-018-1095-9